Parametric study of a high amplitude electromagnetic pulse driven by an intense laser

Aktan, E., Ahmed, H., Aurand, B., Cerchez, M., Poyé, A., Hadjisolomou, P., ... Prasad, R. (2019). Parametric study of a high amplitude electromagnetic pulse driven by an intense laser. Physics of Plasmas, 26(7), [070701]. https://doi.org/10.1063/1.5094871

Published in:
Physics of Plasmas

Document Version:
Peer reviewed version

Parametric study of a high amplitude electromagnetic pulse driven by an intense laser

E. Aktan,[1] H. Ahmed,[2] B. Aurand,[1] M. Cerchez,[1] A. Poyé,[3] P. Hadjisolomou,[2] M. Borghesi,[2] S. Kar,[2] O. Willi,[1] and R. Prasad[1,*]

[1] *Institute für Laser und Plasma Physik, Heinrich Heine Universität Düsseldorf, Universitätsstr.1, D-40225, Germany*
[2] *School of Mathematics and Physics, The Queen's University of Belfast, BT7 1NN, Northern Ireland, UK*
[3] *Centre Lasers Intenses et Applications, University of Bordeaux, CNRS, CEA, Talence 33405, France*

An investigation of the electromagnetic (EM) pulse produced by high intensity laser- solid interaction has been carried out by employing the proton probing technique. Laser parameters including energy, pulse duration and intensity were varied to investigate the influence on the EM pulse amplitude. The data reveal that the amplitude of the EM pulse depends on the incident laser energy and the pulse duration. The optimum pulse length for a given laser energy is found to be close to 100 fs. The net charge associated with the traveling EM pulse has been found to be dependent on the laser intensity, in a good agreement with a semi-empirical model. The understanding of the EM pulse is important for the post acceleration of laser driven proton beams.

PACS numbers: 534

In the last decade, advancement in laser technology has led to a tremendous amount of research work in the field of high intensity laser matter interaction [1–4]. In the near future, the availability of 10 PW class lasers will further thrive an unprecedented quest to study strong field quantum electrodynamics and several nonlinear physics issues, which were inaccessible so far [5]. Already, using existing 100s of TW class lasers, the generation of various types of particle- and radiation sources have been demonstrated, which have significant potential in many scientific and medical applications. In particular, laser driven protons for cancer therapy [6] is one of the most attractive applications being envisioned, albeit characteristics like high repetition rate, stability, high energy and a narrow energy bandwidth need to be addressed.

So far, the most robust acceleration mechanism for laser- driven ions is the target normal sheath acceleration (TNSA) process [7, 8]. The TNSA accelerated ion beams exhibit unique properties such as high laminarity and ultra low emittance. The energy spectrum is however typically broadband, the beam has a large divergence and a lower flux at higher energies. These characteristics limit its potential applications. Numerous experiments with engineered targets have been performed to optimize and control the properties of the ion sources [9–13].

Recently, a technique has been developed, which stands out as a potential scheme not only to control the spectral and angular properties of the proton beams but also to post-accelerate the protons [14]. In a proof of principle experiment at the University of Düsseldorf, an energy gain of more than 50% was achieved resulting in an acceleration gradient of $> 0.5\,\mathrm{GeV/m}$. This acceleration gradient is already well above the level which the conventional accelerators can deliver, and promises a high quality beam as needed for the applications mentioned above. The key ingredient of this technique is the so-called transient electromagnetic (EM) pulse produced by the interaction of a high intensity laser pulse with a solid target that is guided through a miniaturized helical coil. By the intense laser interaction, the electrons are accelerated to MeV energies at the front of the target. A small fraction of the hot electrons can escape the target leading to the build up of a positive potential on the target and hence a neutralizing current is drawn from the ground towards the interaction region. Consequently, a transient EM pulse flows towards the ground.

As discussed in ref. [15], analytical modelling indicates an optimum laser pulse duration and a strong dependence of the EM pulse amplitude on the laser energy. Therefore, a detailed study of the laser parameters affecting the EM pulse is vital for further optimization of the post-acceleration scheme. Furthermore, these studies will also set up a benchmark for the scaling of the acceleration efficiency at short pulse multi-PW laser facilities available for experiments in the near future including the ELI [16] and the APOLLON laser systems [17].

In this letter we report on a parametric study carried out to optimize the strength of the EM pulse generated from a laser solid interaction. Laser parameters such as energy, pulse duration and intensity were varied to quantify the dependence of these parameters on the EM pulse. The experimental data reveal that for 100 fs laser pulses a maximum in the amplitude of the EM pulse is observed. In addition, the dependence on the total charge of the EM pulse associated with the laser intensity is presented, which has been found to be consistent with the estimates of a semi-analytical model employing the ChoCoLaT II code [18].

The experiment was carried out at the ARCTURUS laser facility of the Heinrich-Heine-University of Düsseldorf [19]. The Ti:Sapphire laser system delivers pulses in two beams with energies up to 5 J in each of the beams with a pulse duration of $\sim 30\,\mathrm{fs}$ (FWHM) at the central wavelength of 800 nm. Exploiting this dual beam capability, a pump-probe set-up was used for this experiment. A schematic is shown in Fig. 1(a). One of

*Corresponding author: Rajendra.Prasad@hhu.de

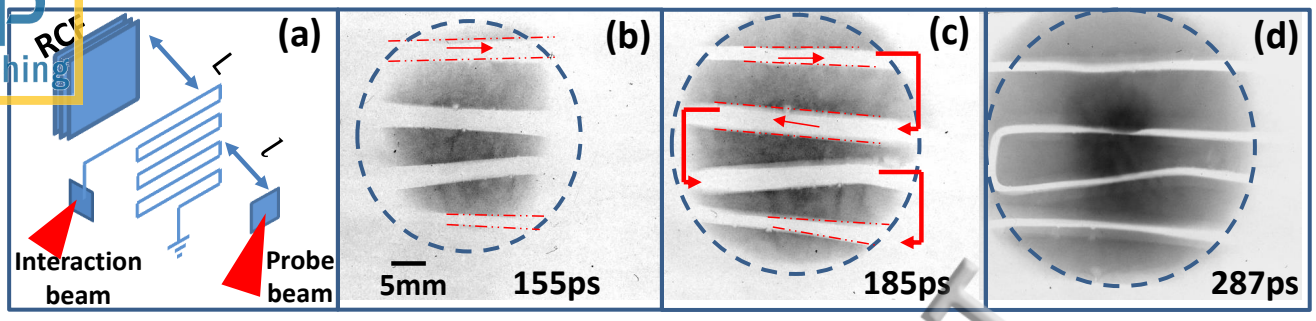

FIG. 1: (Color online) (a) Experimental set-up for the investigation of the EM pulse using proton probing. (b)-(d) Snapshots of the EM pulse flowing along a folded wire towards the ground at different times given by the time of flight of the different energy protons traversing the interaction region. The times mentioned at the bottom right corners correspond to the absolute proton probing timings. In (b) and (c) the solid arrows are the guide to the eye and show the direction of the flow of the EM pulse towards the ground. The dotted lines mark the deflection of the protons from the active (or field) region. For the late probing time (d), the depleted region is very small now as the EM pulse has decayed. The black region encircled by the dotted lines at each layer is the imprint of the proton beam profile.

the beams was focused by an off-axis $f/2$ parabola to a Gaussian focal spot of 5 µm (FWHM), which is hereafter referred to as the "interaction beam". The energy and pulse duration of the interaction beam were varied to investigate their effect on the EM pulse amplitude. The irradiated target was a 10 µm gold foil, attached to an Al wire 100 µm in diameter, which is folded to a square wave pattern (SWP), as shown in Fig. 1(a). This target design allows to keep the EM pulse for a long time in the field of view of the probing proton beam. The second beam was used to accelerate protons from a 10 µm Au foil for probing the EM pulse (hereafter named as "probe beam"). Using an off-axis $f/2$ parabola, the second laser beam was focused to a 4 µm focal spot resulting in an intensity of $I \sim 2 \times 10^{20}$ W/cm^2. The angle of incidence for both laser beams on their respective targets was 25°.

Due to the high laminarity of the proton source, the probing region [20, 21] can be imaged with high spatial resolution in a point projection method. The geometrical magnification of the set-up is given by $M \simeq 1 + L/l$, where L is the distance from the probing plane to the detector and l is the distance from the proton source to the probing plane. For our case, $L = 35 \pm 1$ mm and $l = 4.5 \pm .5$ mm, which gives $M \sim 9$. A stack of radiochromic films (RCF)[22] of the type HD-V2 was used as a detector parallel to the SWP. The two laser beams were timed within a ps by creating a plasma in the air by one of the beams and probing optically by the other beam.

An example of the data of the EM pulse traveling towards the ground along the folded wire is shown in Fig. 1(b-d). Due to the poly-energetic nature of the proton source, images on the three layers are generated by different proton energies such as ~ 3.1 MeV, ~ 4.5 MeV and ~ 5.6 MeV, which correspond to probing times of 155 ps, 185 ps and 287 ps respectively. When the probe protons encounter a region of electrically positive potential, due to the electrostatic force, they are deflected away from the region, creating a depletion of the proton signal in its shadow, and an accumulation of protons at a small distance away from the active region depending on the potential of the region and the energy of the probe protons. Measuring the proton deflection in the radiographs therefore directly reveals the strength of the EM pulse at a given position and time along the probed wire. As the proton deflection also depends on the probe proton energy, the electric field profiles around the wire at different probing times were extracted using the particle-tracing simulation code PTRACE [24]. In this code, the charged particle is traced by solving the equation of motion using a Runge-Kutta fourth-order algorithm, coupled with an adaptive step size monitoring routine. The probed wire was modeled by the PTRACE code using a cylindrical coordinate system. The electric field at any given point, and at a given time, was computed assuming a linear charge density along the wire. A linear charge density profile along the wire for each shot was constructed from the data by following the procedure at different segments of the SWP at different times. The dimensions of the wire were taken from the target images recorded prior to the shot. After the transit of the protons through the field region defined by the wire, the stack detector records the location of every incident proton.

Systematic parametric scans were carried out to explore the effect by varying the laser pulse duration (from 30 fs up to 200 fs) and the laser energy from 90 mJ up to 400 mJ (assuming a 30% energy content within the focal spot of FWHM) on the target. Fig. 2(a) shows the effect of the laser pulse duration on the EM pulse amplitude characterized by the linear charge density profile along the wire. Various laser pulse durations were achieved by detuning the compressor of the interaction beam. As shown, a maximum linear charge density was found at 100 fs for both sets of measurements at laser energies of 300 mJ and 90 mJ on the target. It is interesting to note that the optimum laser pulse duration of ~ 100 fs for the

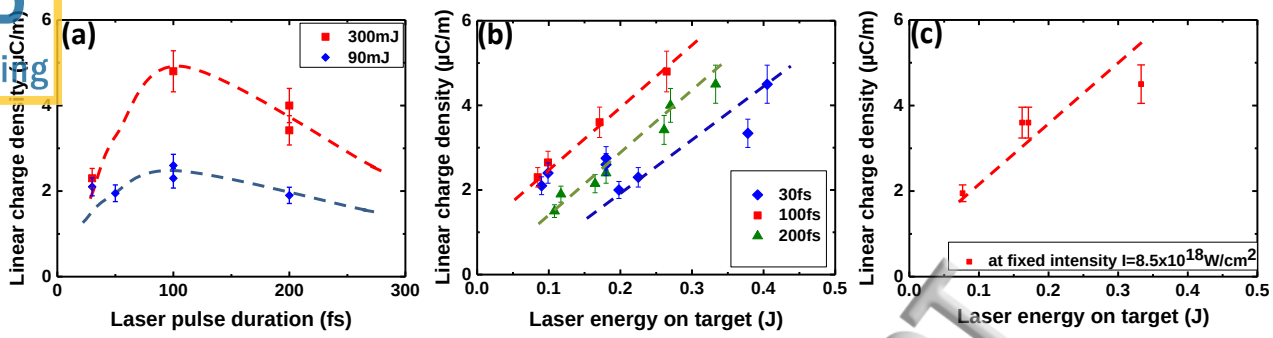

FIG. 2: (Color online) (a) The effect of the laser pulse duration on the linear charge density for two different laser energies on the target: 90 mJ (blue diamond) and 300 mJ (red square). (b) Dependence of the linear charge density on the laser energy at three pulse durations: 30 fs (blue diamond), 100 fs (red square) and 200 fs (olive triangle). (c) The dependence of the linear charge density on the laser energy at a fixed intensity of 8.5×10^{18} W/cm^2. Here the intensity of the pulse is kept the same by changing both the laser energy and the pulse duration. The error bars account for the inaccuracy in calculating the amplitude of the EM pulse. The dotted lines in (a) and (c) are guides to the eyes. The dotted lines in (b) are a linear fit.

generation of a strong EM pulse amplitude is consistent with the model presented in refs [15, 27]. In Fig. 2(b), the linear charge density is plotted against the laser energy for three different laser pulse durations viz. 30 fs, 100 fs and 200 fs. This graph illustrates the effect of the laser energies on the amplitude of the EM pulse. As can be seen in Fig. 2(b), the linear charge density at a given laser pulse duration increases linearly with the laser energy for our energy range. A more generic trend based on an analytical estimate, for a wide range of energies is discussed later.

Based on the phenomenological model discussed in ref. [15], the hot electron spectrum produced by the laser interaction plays an important role in describing the dynamics and the relationship between the laser parameters and the net charge escape. An exponential electron spectrum can be assumed of the form, $dN/dE = (N_0/U_\mathrm{p})\exp(-E/U_\mathrm{p})$, where E is the electron energy, $U_p = \mathrm{k_B}T_\mathrm{e}$ is the ponderomotive potential of the incident laser pulse, $\mathrm{k_B}$ is the Boltzmann's constant and T_e is the hot electron temperature. N_0 is the total number of hot electrons produced by the interaction given as $N_0 = \eta E_L/U_P$ assuming an exponential spectrum, where E_L is the laser energy on the target and η is the laser to electron conversion efficiency. For a finite size of the target, the charging up reaches a saturation depending on the target self-capacitance (C_tar). This effect can be taken into account by calculating the potential barrier (ϕ) for the escaping electrons. Mathematically, one can write the number of escaping electrons as

$$N_{esc} = (\eta E_L/U_p)\ exp(-e\phi/U_p), \tag{1}$$

where ϕ is obtained from the energy balance equation

$$eN_{esc}/C_\mathrm{tar} = \phi \tag{2}$$

Considering $eN_{esc} = Q = \int_{-\infty}^{\infty} \lambda dl$, where λ is the linear charge density per unit length, typically obtained in our experiment (~ 60 nC [15]), for instance,

$$\phi = Q/C_\mathrm{tar} = Q/(8\varepsilon_0 r_\mathrm{tar}) \ \sim 0.9\,\mathrm{MeV}. \tag{3}$$

Here ε_0 is the free space permittivity and $r_\mathrm{tar} = 1.15$ mm, is the radius of the foil target assuming a circular disc equivalent to a square shaped target of $\sim 2.3 \times 2.3\,\mathrm{mm}^2$ as used in the experiment. This potential is significantly smaller than the hot electron temperature in our case which is estimated to be a few MeV using the ponderomotive scaling [7]. It is therefore reasonable to assume that the target size does not affect the electron escape. Under this condition, i.e for a sufficiently high electron temperature such that $e\phi < U_P$, increasing the laser energy simply would lead to an enhanced charge accumulation at a fixed laser pulse duration. Assuming the typical $I^{1/2}$ scaling for the hot electron temperature [1], one can express the equation 1 as $N_{esc}(E_L) \sim k_1\sqrt{E_L}(1 - k_2\phi/\sqrt{E_L})$, where k_1 and k_2 are constants for this equation. Equation 2 therefore suggests that the target potential scales with $\sqrt{E_L}$ which implies, by substituting in the above expression for $N_{esc}(E_L)$. Consequently, the target charge also scales with $\sqrt{E_L}$ which is in broad agreement with the data shown in Fig. 2(b). As shown later in this paper, this also agrees well with the results obtained from simulations based on a more detailed modeling of the highly dynamic process of the target charging following the laser interaction.

When decreasing the intensity at a given energy, for instance by increasing the pulse duration, the total number of electrons (N_0) produced by the interaction is enhanced with a lower average energy. Consequently, this increases the net escaping charge Q and the target potential ϕ. However for sufficiently low intensities the average electron energy is less than the target potential. The net escaping charge starts to drop as there are fewer hot electrons surpassing the potential barrier. For a given laser

energy and varying intensity, equation 1 indicates that the number of escaping electrons (N_{esc}) will be maximum for $e\phi_0 = U_p$, which yields the condition for maximum electron escape, U_p [in MeV] $= \sqrt{0.37\ \eta E_L / C_{\rm tar}}$[in pF]. Considering a prudent 30% laser-electron conversion efficiency [25, 26], the optimum electron temperature for a 300 mJ laser energy is ∼700 keV in our case which corresponds to a laser pulse duration of ∼ 150 fs, in broad agreement with the data shown in Fig. 2(a).

The electrical charging of the target during the interaction is a highly dynamic process, which is self-consistently governed by the temporally evolving target potential due to the escape of the hot electrons. The collisional cooling of the hot electrons inside the target can, in principle, lead to a significant loss of the electron mean energy over several ps of the charging period. Hence, it plays an important role for long pulse durations ($\gtrsim$ ps), as suggested by the model presented in [18, 27]. The cooling time of electrons can be obtained using the hot electron temperature and the stopping range of the electrons.

The maximal range reached by the electrons (with an energy of 3.3 MeV) is calculated by using data from ESTAR [28] which gives a stopping range of 1.1 mm. Based on these parameters, a prudent estimation is ∼ 0.5 ps, for the cooling time in our case which is significantly longer than the laser pulse durations discussed here. Therefore, it is reasonable to neglect electron cooling in the observed linear charge density shown in Fig. 2(b).

In order to decouple the effect of the laser intensity from the laser energy, both the laser energy and the pulse duration were varied which provided a set of data for the linear charge density at a fixed intensity, as shown in Fig. 2(c). Although the laser intensity was the same for all the four data points, the linear charge density increased almost linearly with the laser energy on the target. This implies that for a given ponderomotive potential (i.e. for a given temperature of the hot electron population produced by the interaction), a higher laser energy of the pulse increases the flux of the hot electrons, hence, the net escaping electrons.

Fig. 3(a) illustrates the effect of the laser intensity on the total charge of the EM pulse for three laser pulse durations. The total charge in the EM pulse is calculated by considering an EM pulse duration of 25 ps (FWHM), as reported in refs [15, 29], for ps and fs lasers. In addition, a data point (the magenta circle) is shown from a previous measurement [15] performed at the ARCTURUS laser system, which corresponds to a pulse of 30 fs, 1 J and an intensity of $I \sim 10^{20}$ W/cm^2. Moreover, as shown in Fig. 3(a), the total charge in the pulse calculated from the experimental data agrees well with that estimated by the semi-analytical model of target charging reported in ref. [18], employing the ChoCoLaT II code. The total charge scales as $I^{0.54}$, similar to that predicted by the phenomenological model discussed earlier.

Motivated by the agreement between the experiment and the simulations, a systematic parametric scan for the total charge was carried out using the ChoCoLaT II code for a range of laser energies and pulse durations as shown in Fig. 3(b). As can be seen from this parametric map, the total amount of charge contained in the EM pulse gradually increases with the laser energy, however, there exists an optimum pulse duration for a given laser energy. The solid black line highlights the laser pulse durations for different laser energies that optimize the

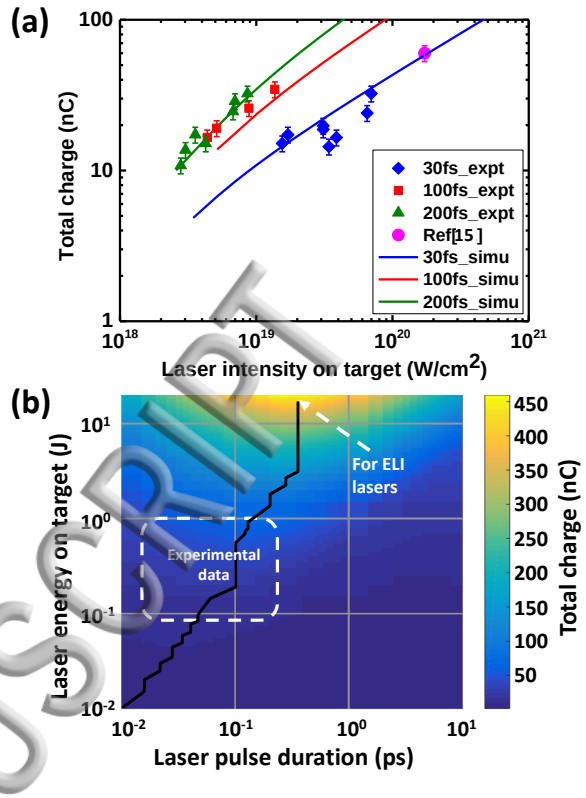

FIG. 3: (Color online)(a) The dependence of the total charge contained in the EM pulse on the laser intensity at three different laser pulse durations viz. 200 fs (olive triangle), 100 fs (red square) and 30 fs (blue diamond). The point shown in magenta is the data from the previous measurement reported in ref. [15], where the laser pulse duration was 30 fs and the laser energy was 1 J on the target. The solid lines with corresponding colors of the experimental data, are obtained from the ChoCaLaT II code. (b) A parametric scan is shown of the total charge by varying the laser energy and the pulse duration, using the ChoCoLaT II code. The dashed square represents the parameter range covered by the current and previous experiments. The solid black line represents the laser pulse durations to maximize the total charge for a given laser energy. The arrow indicates the optimum pulse duration for the ELI-class lasers. Due to the extended range of the pulse durations and energies used in this scan, the step size on each axis was varied ensuring a good resolution. On the time axis, for the time intervals [10 fs, 100 fs], [100 fs, 1 ps] and [1 ps, 10 ps], the simulation step sizes were 5 fs, 50 fs and 500 fs, respectively. Similarly, on the energy axis, the step sizes for the energy ranges [10 mJ, 100 mJ], [100 mJ, 1 J] and [1 J, 20 J], were 5 mJ, 50 mJ and 0,5 J respectively. The target thickness used in all these simulations was 10 µm Au, as used in the experiment.

total charge in the EM pulse. The area covered by the dashed square represents the parameter range covered so far in the experiments, whereas an optimum pulse duration of a few 100 fs (as pointed out in the figure.) is predicted by the simulations for the upcoming lasers including the ELI-Beamlines, ELI-NP [30]. As discussed in refs.[14, 15], an efficient post-acceleration of ions can be achieved by harnessing the EM pulse via helical coil targets. The strength of the longitudinal accelerating field inside the coil target is directly proportional to the strength of the EM pulse, i.e. the higher the amplitude of the EM pulse the larger the acceleration gradient for the post-acceleration of the proton beams. Therefore, it would be highly favorable to use a laser pulse duration at an optimum for a given laser energy on the target to maximize the total charge Q in the EM pulse.

In summary, we have performed a detailed study of the EM pulse amplitude by changing the laser parameters. The experimental results suggest that the EM pulse amplitude has a maximum for a laser pulse duration of around 100 fs and the amplitude increases with the laser energy for a given pulse duration. The total charge associated with the EM pulse for different laser pulse durations fits well with the simulations using the ChoCoLaT II code. The optimum laser pulse duration over a large range of energies and pulse lengths was obtained from the simulations. The simulations predict the optimum pulse duration for the upcoming laser facilities allowing the maximum charge to be achieved. These studies represent a significant step forward towards understanding the dynamics of the EM pulse generation, and indicate a route for optimization required by the post-acceleration using helical coils for laser-driven protons.

Acknowledgments

The research was supported by the DFG Transregio SFB/TR18 (project-5486099) program of Germany. Co-authors also acknowledge the support from the EPSRC, UK for the projects EP/L002221/1, EP/K022415/1 and EP/I029206/1.

[1] A. Macchi, M. Borghesi and M. Passoni, Review Modern Phys. **85**, 751 (2013).
[2] V. Malka, J. Faure, Y. A. Gauduel, E. Lefebvre, A. Rousse and K. T. Phuoc, Nat. Phys. **4**, 447 (2008).
[3] J. Fuchs, P. Antici, E. d'Humiéres, E. Lefebvre, M. Borghesi, E. Brambrink, C. A. Cecchetti, M. Kaluza, V. Malka, M. Manclossi, S. Meyroneinc, P. Mora, J. Schreiber, T. Toncian, H. Pépin and P. Audebert, Nat. Phys. **2**, 48 (2006).
[4] L. Robson, P. T. Simpson, R. J. Clarke, K. W. D. Ledingham, F. Lindau, O. Lundh, T. McCanny, P. Mora, D. Neely, C. -G. Wahlström, M. Zepf and P. McKenna, Nat. Phys. **3**, 58 (2007).
[5] A. Di Piazza, C. Müller, K. Z. Hatsagortsyan, and C. H. Keitel, Rev. Mod. Phys. **84**, 1177 (2012).
[6] S.V. Bulanov, T.Zh. Esirkepov, V.S. Khoroshkov, A.V. Kuznetsov, F. Pegoraro, Phys. Lett. A **299**, 240 (2002).
[7] S. C. Wilks, A. B. Langdon, T. E. Cowan, M. Roth, M. Singh, S. Hatchett, M. H. Key, D. Pennington, A. MacKinnon and R. A. Snavely, Phys. Plasmas **8**, 542 (2001).
[8] E. L. Clark, K. Krushelnick, J. R. Davies, M. Zepf, M. Tatarakis, F. N. Beg, A. Machacek, P. A. Norreys, M. I. K. Santala, I. Watts and A. E. Dangor, Phys. Rev. Lett. **84**, 670 (2000).
[9] T. Toncian, M. Borghesi, J. Fuchs, E. d'Humiéres, P. Antici, P. Audebert, E. Brambrink, C. A. Cecchetti, A. Pipahl, L. Romagnani and O. Willi, Science **312**, 410 (2006).
[10] B. M. Hegelich, B. J. Albright, J. Cobble, K. Flippo, S. Letzring, M. Paffett, H. Ruhl, J. Schreiber, R. K. Schulze, J. C. Fernandez, Nature **439**, 441 (2006).
[11] M. Gauthier, J. B. Kim, C. B. Curry, B. Aurand, E. J. Gamboa, S. Göde, C. Goyon, A. Hazi, S. Kerr, A. Pak, A. Propp, B. Ramakrishna, J. Ruby, O. Willi, G. J. Williams, C. Rödel and S. H. Glenzer, Review of Scientific Instruments **87**, 11D827 (2016).
[12] I. Prencipe, J. Fuchs, S. Pascarelli, D. W. Schumacher, R. B. Stephens, N. B. Alexander, R. Briggs, M. Büscher, M. O. Cernaianu, A. Choukourov et al., High Power Laser Science and Engineering **5**, 1 (2017).
[13] P. Hilz, T. M. Ostermayr, A. Huebl, V. Bagnoud, B. Borm, M. Bussmann, M. Gallei, J. Gebhard, D. Haffa, J. Hartmann et. al., Nat. Commun **9**, 423 (2018).
[14] S. Kar, H. Ahmed, R. Prasad, M.Cerchez, S. Brauckmann, B. Aurand, C. L. S.Lewis, A. Macchi, G. Nersisyan, G. Cantono, P. Hadjisolomou, A. P. L. Robinson, A. M. Schroer, M. Swantusch, M. Zepf, O. Willi and M. Borghesi, Nat. Commun **7**, 10792 (2016).
[15] H. Ahmed, S. Kar, G. Cantono, P. Hadjisolomou, A. Poye, D. Gwynne, C. L. S. Lewis, A. Macchi, K. Naughton, G. Nersisyan, V. Tikhonchuk, O. Willi and M. Borghesi, Sci. Report **7**, 1 (2017).
[16] https://eli-laser.eu.
[17] https://portail.polytechnique.edu/luli/en/cilex-apollon/apollon
[18] A. Poyé, S. Hulin, J. Ribolzi, M. Bailly-Grandvaux, F. Lubrano-Lavaderci, M. Bardon, D. Raffestin, J. J. Santos, and V. Tikhonchuk Phys. Rev. E **98**, 033201 (2018).
[19] O. Willi, M. Behmke, L. Gezici, B. Hidding, R. Jung, T. Königstein, A. Pipahl, J. Osterholz, G. Pretzler, A. Pukhov, M. Toncian, T. Toncian, M. Heyer, O. Jäckel, M. Kübel, G. Paulus, C. Rödel, H. P. Schlenvoigt, W. Ziegler, M. Büscher, A. Feyt, A. Lehrach, H. Ohm, G. Oswald, N. Raab, M. Ruzzo, M. Seltmann and Q. Zhang Plasma Phys. Control. Fusion **51**, 124049 (2009).
[20] M. Borghesi, D. H. Campbell, A. Schiavi, M. G. Haines, A. J. MacKinnon, P. Patel, L. A. Gizzi, M. Galimberti, R. J. Clarke, F. Pegoraro, H. Ruhl, S. Bulanov and O. Willi, Phys. Plasmas **9**, 2214 (2002).

[21] L. Romagnani, J. Fuchs, M. Borghesi, P. Antici, P. Audebert, F. Ceccherini, T. Cowan, T. Grismayer, S. Kar, A. Macchi, P. Mora, G. Pretzler, A. Schiavi, T. Toncian, and O. Willi, Phys. Rev. Lett. **95**, 195001 (2005)
[22] M. J. Butsona, P. K. N. Yua, T. Cheunga, P. Metcalfe, Materials Science and Engineering R **41**, 61 (2003).
[23] J. F. Ziegler, SRIM-2013 Available at: www.srim.org.
[24] A. Schiavi, PhD thesis, Imperial College of Science, Technology and Medicine, London, UK (2003).
[25] G. Malka and J. L. Miquel, Phys. Rev. Lett. **77**, 75 (1996).
[26] K. B. Wharton, S. P. Hatchett, S. C. Wilks, M. H. Key, J. D. Moody, V. Yanovsky, A. A. Offenberger, B. A. Hammel, M. D. Perry and C. Joshi et al. Phys. Rev. Lett. **81**, 822 (1998).
[27] A. Poyé, J. L. Dubois, F. L. Lavaderci, E. d'Humiéres, M. Bardon, S. Hulin, M. B. Grandvaux, J. Ribolzi, D. Raffestin, J. J. Santos, Ph. Nicolaï and V. Tikhonchuk, Phys. Rev. E **92**, 043107 (2015).
[28] https://physics.nist.gov/PhysRefData/Star/Text /ESTAR.html
[29] H. Ahmed, S. Kar, G. Cantono, G. Nersisyan, S. Brauckmann, D. Doria, D. Gwynne, A. Macchi, K. Naughton, O. Willi, C. L. S. Lewis, M. Borghesi, Nuclear Instruments and Methods in Physics Research A **829**, 172-175(2016).
[30] http://www.eli-np.ro/

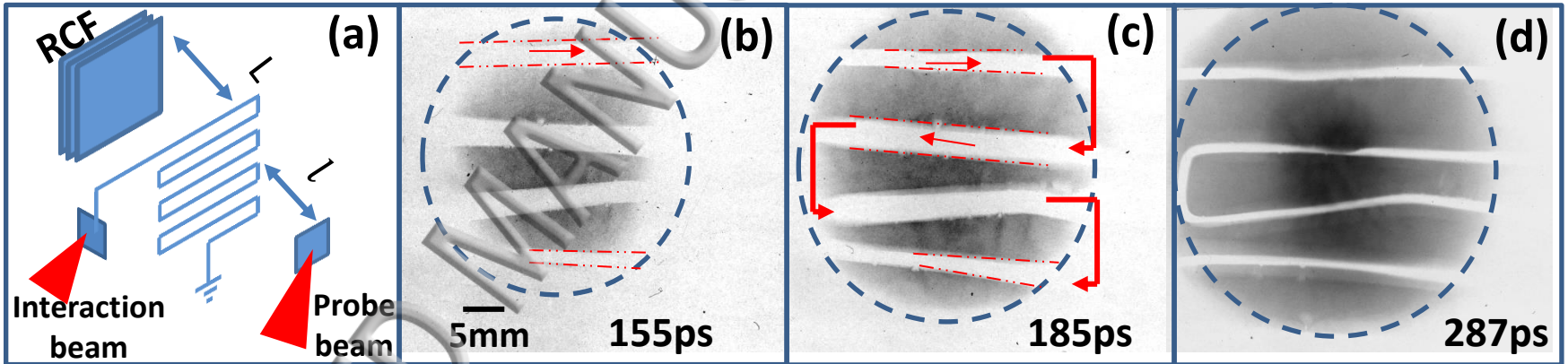
RCF
L
L
(a)
Interaction beam
Probe beam
(b)
5mm
155ps
(c)
185ps
(d)
287ps

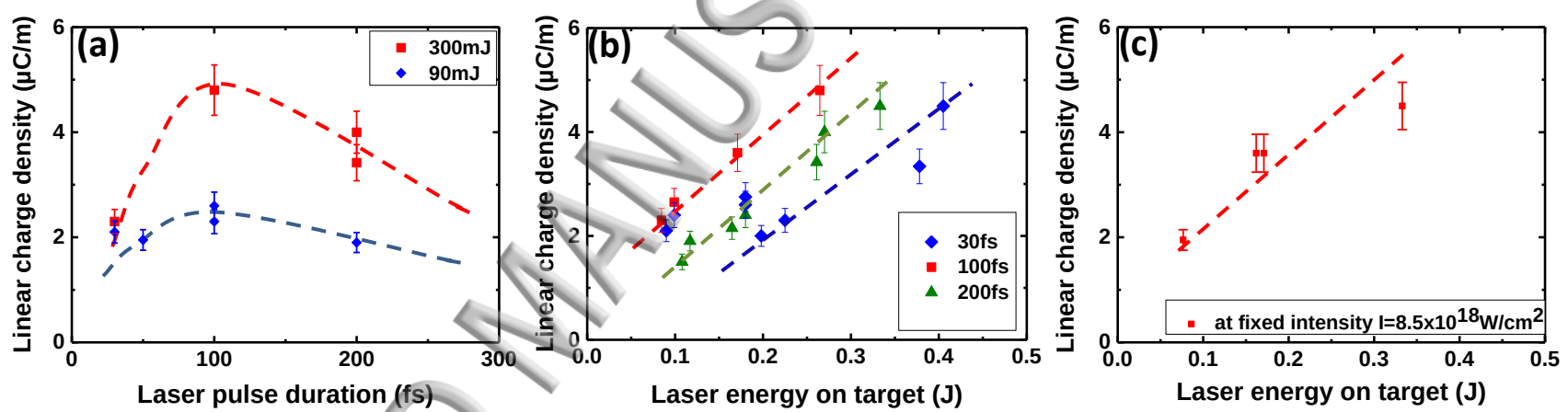
(a)
300mJ
90mJ
Linear charge density (μC/m)
Laser pulse duration (fs)
(b)
30fs
100fs
200fs
Linear charge density (μC/m)
Laser energy on target (J)
(c)
at fixed intensity I=8.5x10^18W/cm^2
Linear charge density (μC/m)
Laser energy on target (J)

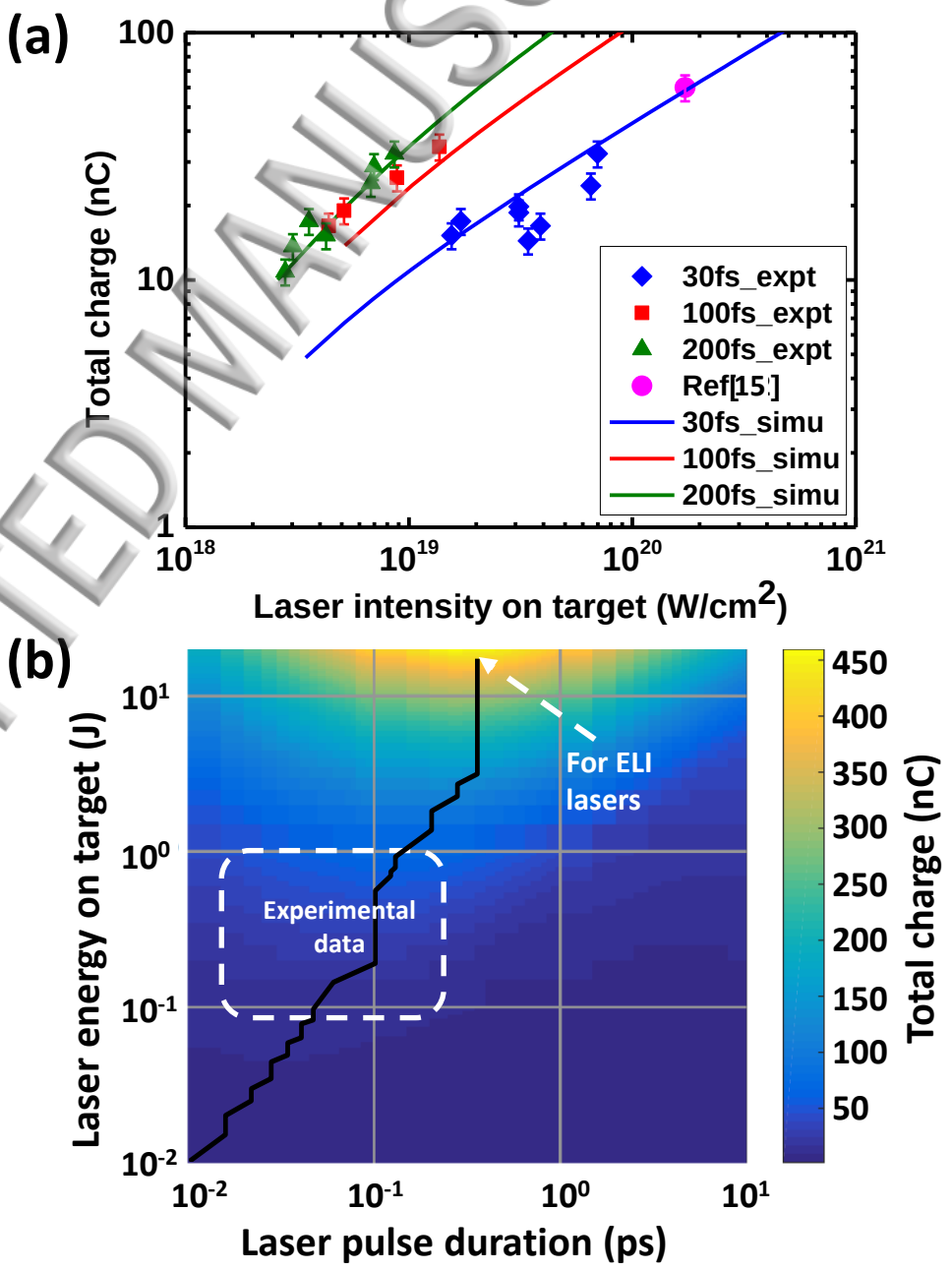
(a)
100
10
1
Total charge (nC)
10^{18}
10^{19}
10^{20}
10^{21}
Laser intensity on target (W/cm^2)
30fs_expt
100fs_expt
200fs_expt
Ref[15]
30fs_simu
100fs_simu
200fs_simu
(b)
10^{1}
10^{0}
10^{-1}
10^{-2}
Laser energy on target (J)
For ELI lasers
Experimental data
10^{-2}
10^{-1}
10^{0}
10^{1}
Laser pulse duration (ps)
450
400
350
300
250
200
150
100
50
Total charge (nC)